Chapter 8
Types of Nanomaterials and Their Properties

8.1 Introduction

It is an interesting question as to, starting with a few atoms, how the bulk materials reach their structure and related properties. Do they undergo any structural changes or even their smallest unit cell is similar to that in bulk material? This question has been addressed by many. There are reasons to believe that the small clusters or nanoparticles are not just the fragments of bulk materials. There can be entirely different structures as well as bonds and bond strengths in clusters which can even differ from nanomaterials.

It has been well established now that all the materials, may be metals, semiconductors or insulator clusters or nanomaterials, have size dependent physicochemical properties. In most of the cases a cluster size is below 1 nm and that of nanoparticles is in the 1–100 nm range. Interestingly at such a small size even the shape of the material and interactions between clusters or nanomaterials decide the properties of the material. This opens up a huge possibility of tailor making the materials, which have different properties just due to their size, shape and/or assembly. In this chapter we will discuss to some extent clusters, semiconductor metal nanomaterials and magnetic nanomaterials. Nanomaterials would mean 0-D, 1-D or 2-D materials with the relevant dimensions smaller than $\sim$100 nm to qualify them as nanomaterials. The general analysis methods for all the nanomaterials are as mentioned in Chap. 7. In this chapter some additional relevant analysis is discussed for semiconductor and metal nanoparticles. The chapter closes with some additional properties like mechanical, structural, electrical and thermal properties of the nanomaterials in general.

S.K. Kulkarni, *Nanotechnology: Principles and Practices*,
DOI 10.1007/978-3-319-09171-6_8

8.2 Clusters

Clusters are aggregates of small number of atoms and can be considered as intermediates of atoms and nanomaterials. Depending upon the number of atoms they can be roughly divided into following:

1. Microclusters – number of atoms between 2 and 10–13 atoms
2. Small clusters – number of atoms between 10 and 13 to about 100 atoms
3. Large clusters – number of atoms between about 100 and 1,000 atoms.

With number of atoms larger than 10^3 and below 10^6 atoms it is a nano-particle. Although the classification of clusters and nanomaterials cannot be very precise, usually clusters are smaller than $\sim$1 nm.

One may also ask the question, what is the difference between a large atom, small molecule with couple of atoms and a cluster? For example a 92-atom sodium atom cluster and uranium atom with atomic number 92. A sodium atom cluster with one valence electron and 92 free electrons of sodium atom would make it appear like a uranium atom. However, in uranium atom the positive charge is concentrated in the nucleus in a very small volume and 92 electrons have some specific electron configuration. On the other hand, in a sodium atom cluster, each atom's positive charge is spatially separated from the other atoms and each one would have its ionic shell configuration; only 92 electrons would be free to form an electron gas of the cluster. As far as molecules are concerned they have stable configuration of certain types and number of atoms. They have fixed composition, structure, bond lengths, bond angles and, hence, fixed properties. The clusters on the other hand are the aggregates of atoms and may or may not be stable. The structure, bonds etc. vary with number of atoms and so do the properties. In clusters large fraction of atoms is on the surface. For example in a cluster of 55 atoms like that of argon or sodium 32 atoms are on the surface and only 23 are inside. Often we are only able to understand their presence in some experiments but may not be able to collect them. However, their theoretical as well as experimental investigations can lead to the understanding of the basic processes that take place while the clusters are formed and also lead to applications in catalysis, epitaxial materials and so on.

8.2.1 Types of Clusters

Besides the classification of clusters depending upon the number of atoms they contain, it is possible to realize various types of clusters as follows:

1. Homogeneous clusters – containing only single type of elements, e.g. Ar, Na, K, Si, Au, Pb etc.
2. Heterogeneous clusters – $3Na + 3K$, $2Na + 3K$ etc. $(NaCl)_n$ or Na_nCl_{n+y}, $(Na_{n+1}Cl_n)^+$, $(Na_nCl_{n+1})^-$ and many other kinds and compositions.

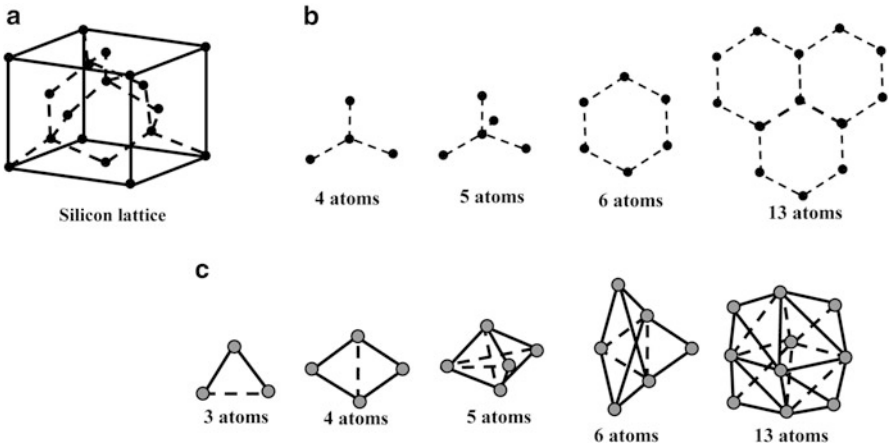

Fig. 8.1 (**a**) Silicon atoms forming a unit cell, (**b**) fragments of silicon unit cell, and (**c**) stable clusters of silicon

3. Oppositely charged clusters may be attracted and stay together.
4. Covalently bonded clusters like carbon, silicon etc. Fullerenes or C60 atom clusters are examples of such clusters and will be discussed in Chap. 9.

In a silicon cluster, the stable configurations are not the fragments of bulk lattice and instead of having 4, 5, 6 atoms in clusters, stable clusters having 3, 4 ... atoms with different structure rather than bulk fragmentation are energetically favoured (Fig. 8.1) (Box 8.1).

Box 8.1: Clusters and Platonic Solids

A cluster may be considered as being formed shell by shell around a central atom. As the number of shells increase, total number of atoms goes on increasing and percentage of surface atoms compared to interior goes on decreasing. The magic number of atoms in a cluster can be obtained by first considering some basic types which were formulated by ancient mathematicians like Pythagoras and Plato around 450 B.C. The basic shapes considered were cube, octahedron, icosahedrons, tetrahedron and dodecahedron related to earth, air, water, fire and heavenly constellation respectively. One of the common metal cluster is 13-atom icosahedrons. It has one central atom and 12 surrounding atoms, 20 faces, 12 vertices and 30 edges. Number of atoms in the nth shell of an icosahedron can be obtained from $10\,n^2+2$.

Figure 8.2 shows few icosahedrons clusters.

(continued)

Box 8.1 (continued)

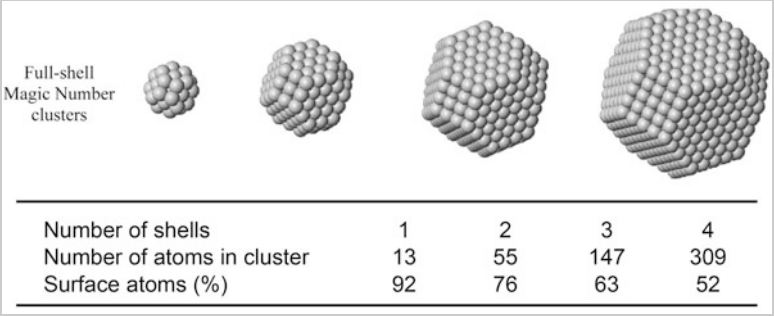

Number of shells	1	2	3	4
Number of atoms in cluster	13	55	147	309
Surface atoms (%)	92	76	63	52

Fig. 8.2 Icosahedron clusters with complete shells

5. Metal atom clusters i.e. a phase in which they would ultimately develop if the cluster and nanoparticle size is exceeded. In fact even before a material reaches a bulk size with some critical number of atoms characteristic of the material it undergoes various transitions assuming local stable sizes. This has been very well exemplified for potassium clusters (see Fig. 8.3). Here the ionization energy is plotted as a function of the number of atoms in a cluster. More the ionization energy more stable is the cluster. One can see that 8, 18, 20 ... atoms clusters are locally stable compared to the other neighbouring clusters. After having about 92

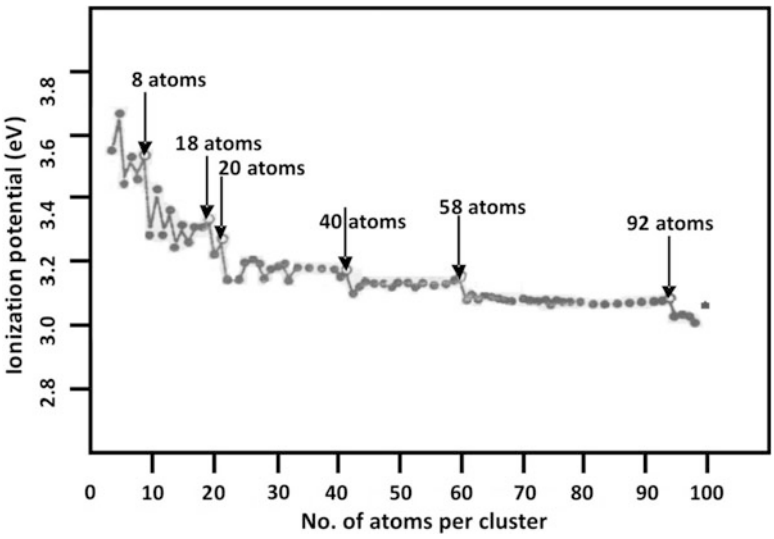

Fig. 8.3 Variation of ionization energies of different potassium clusters having different number of atoms in them

atoms, the cluster reaches the ionization potential (or work function value) of a bulk potassium metal. The clusters also can have different structures compared to the bulk material. One can get more insight about the metal clusters by using a jellium model.

6. Clusters of rare gases – close shell atom clusters of Ar, Kr etc. are held together by weak van der Waals forces and formed at low temperatures.
7. Clusters with hydrogen bonds, for example a $(H_2O)_n$ cluster. It is a strongly held molecular cluster, stronger than cluster of rare gases but much weaker than metallic, covalent or ionic clusters.
8. Magnetic clusters – clusters of atoms with resultant magnetic moment. The magnetic moments on clusters like Co, Fe and Ni may show the moment close to magnetic moment/atom.

Usually shell theory applies to atoms, nuclei as well as clusters. In all the three cases fermions are confined in $\sim 10^{-12}$ cm for nuclei, 10^{-8} cm for atoms and $\sim 10^{-7}$ to 10^{-6} cm in case of clusters. Using appropriate angular momentum conditions for the spherical harmonic, square well or spherical potential shells are developed which are a direct result of application of quantum mechanics. In all these cases interacting fermions obeying Pauli exclusion principle result ultimately to shells with magic numbers or in case of clusters some stable clusters are referred to as 'magic clusters'.

In order to obtain very small clusters, starting with 2–3 atoms upto few tens of atoms, special, very sophisticated machines are built. Usually an intense beam of laser is made incident on a bulk piece of material whose clusters are to be investigated. The evaporation normally contains clusters of different sizes which need to be mass selected using a mass spectrometer. The mass selected cluster would then have abundance of clusters of uniform size (same number of atoms per cluster). Such a cluster is then fragmented by another beam of laser which is then analyzed with another mass spectrometer. This analysis would then lead to the understanding of stability of the clusters. For example, if a four-atom cluster is less stable than a three-atom cluster, the fragmentation should show the abundance of three-atom clusters than four-atom clusters.

In some cases where ionization of the clusters is investigated, an oven is used as a source of clusters, where the source material from the hot oven is expanded through a nozzle, ionized in a chamber using photons or electron beam and then analyzed using a mass spectrometer. Of course in both the types of apparatus discussed here, adequate vacuum system is a must in order to avoid any contaminations.

8.3 Semiconductor Nanoparticles

Every material has a characteristic size below which size dependent properties are realized. In semiconductors this size is nothing but the size of the exciton. Understanding the concept of exciton and estimating its size for different semiconductor materials is the first step towards understanding the semiconductor nanoparticles.

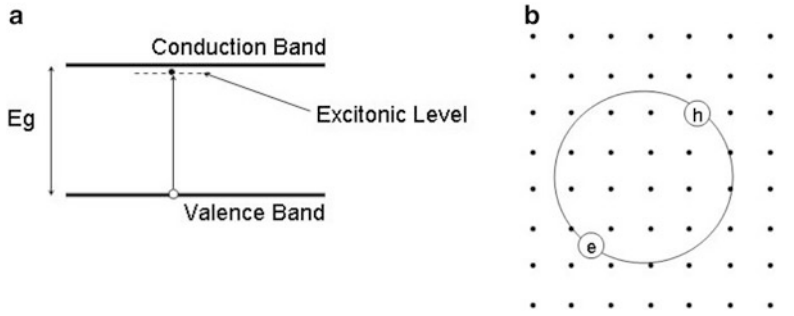

Fig. 8.4 (**a**) Energy level diagram for a typical semiconductor along with the excitation energy level. (**b**) Mott-Wannier exciton in a typical lattice

8.3.1 Excitons

In semiconductor or insulator, valence and conduction bands are separated by some finite energy gap characteristic of the material. When an electron from the valence band gets sufficient energy to overcome the energy gap, may be by thermal excitation or absorption of photon, and go to conduction band, a hole is left behind. The electron-hole pair so formed is a quasi-particle called exciton (see Fig. 8.4). An exciton, whose centre of mass motion is quantized, can move in the crystal.

Different kinds of excitons are identified in a variety of materials. Note that the spins of electron and hole in an exciton pair can be either parallel or antiparallel to each other. If the spins of hole and electron in an exciton are parallel to each other the 'dark exciton' results and 'bright exciton' otherwise. The properties of dark and bright excitons are different. As its name suggests dark exciton is optically inactive but the bright exciton is optically active. The optical exciton is useful in optical sensing and emission. Dark exciton, one may think, would not be useful. However, dark excitons and bright excitons can be interchanged by spin flip-flop and this has potential application in spin storage and qbits.

Depending upon the intensity of the light used to excite the excitons, it is also possible under intense illumination that a large number of excitons (exciton liquid) are formed which start interacting with each other. Two interacting excitons can attract each other forming a 'biexciton'. One can write

$$\delta E_{\text{exc}} = E_{\text{biexc}} - 2E_{\text{exc}} \tag{8.1}$$

Here E_{exc} is the energy of a single exciton, E_{biexc} is the energy of the two interacting excitons and δE_{exc} is the difference in the energies given by equation 8.1. Obviously the bound pair will be formed if the energy $\delta E_{\text{exc}} < 0$. Although there is a lot of interesting research being carried out to study the lifetime, dynamics and optical properties of biexcitons, we will not go into more depth here as it is beyond the scope of this book.

We shall consider here single (or widely isolated), optically active excitons. When the electron-hole pair is tightly bound with distance between electron and hole comparable to the lattice constant of the material, it is called Frenkel exciton. At the other extreme, one may have an exciton with electron-hole separation much larger compared to the lattice constant. Such a weakly bound electron-hole pair is called as Mott-Wannier exciton. The energy of such an exciton is slightly less than the energy gap (E_g) between valence and conduction band. In fact the energy gap E_g can be also defined as the energy necessary to create a free electron and a free hole. The Hamiltonian for Mott-Wannier exciton is given as

$$H = \frac{P_e^2}{2m_e} + \frac{P_h^2}{2m_h} - \frac{e^2}{\varepsilon |r_e - r_h|} \tag{8.2}$$

where m_e and m_h are effective electron and hole mass respectively, and ε is the dielectric constant of semiconductor material. It should be remembered that the mass of an electron and hole in a solid material and even a nanomaterial is not same as that of a 'free electron' mass. It may be smaller or larger than the free electron mass depending upon the curvature of a band. For more details one should refer to a text book on Solid State Physics. First two terms on the right hand side of Eq. (8.2) are kinetic energies of electron and hole respectively and the third term is the Coulomb energy of electron-hole attraction or potential energy.

The Bohr radius of such an exciton is given as

$$r_B = \frac{\hbar^2 \varepsilon}{e^2} \left[\frac{1}{m_e} + \frac{1}{m_h} \right] \tag{8.3}$$

In Table 8.1 radii for few semiconductor spherical nanoparticles are illustrated.

It may be noticed that these values of r_B are of the order of a few nanometres. We observe in a nanoparticle and other nanostructures a situation in which exciton is confined in the nanostructure. The sizes of excitons are often comparable to the sizes of nanoparticles or nanostructures.

8.3.2 *Effective Mass Approximation*

There are various theories like Effective Mass Approximation (EMA) and Tight Binding (TB) developed to explain the size dependent energy gap variation (being most important property of semiconductor materials on which other properties

Table 8.1 Bohr radius (r_B) for exciton in some semiconductors

Semiconductor	E_g (eV)	m_e	m_h	ε	r_B (nm)
GaAs	1.52	0.067	0.082	13.1	18.8
InP	1.42	0.077	0.64	12.4	9.6
InSb	0.24	0.0145	0.39	17.6	66.7

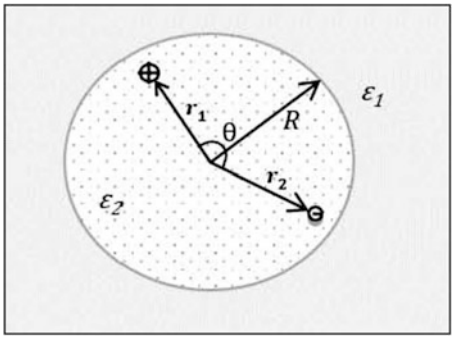

Fig. 8.5 Spherical semiconductor nano-particle embedded in a medium with different dielectric medium

depend) in nanostructures. Depending upon the material or group of materials one theory may be more applicable than the other. Nonetheless, EMA works out to be reasonably well in most of the cases. It nicely explains the dependence of energy gap opening with the reduction of size and will be discussed here. Historically, Efros and Efros first formulated this theory which was extensively developed by L.E. Brus. Briefly it is outlined below.

Consider a dielectric sphere with dielectric constant ε_2 embedded in a medium of dielectric constant ε_1. Let the radius of the sphere be R (see Fig. 8.5).

If $\mathbf{r}_1$ and $\mathbf{r}_2$ are the positions of the charges inside the sphere, the potential energy can be written as

$$V\left(\mathbf{S}_1,\ \mathbf{S}_2\right) = \pm\frac{e^2}{\varepsilon_2\left|\mathbf{r}_1-\mathbf{r}_2\right|} + \mathbf{P}\left(\mathbf{r}_1\right) \pm \mathbf{P}\left(\mathbf{r}_2\right) \pm \mathbf{P}_M\left(\mathbf{r}_1,\ \mathbf{r}_2\right) \tag{8.4}$$

where polarization $\mathbf{P}$ is given as

$$\mathbf{P}\left(\mathbf{r}\right) = \sum\nolimits_{n=0}^{\infty}\alpha_n\left(\frac{r}{R}\right)^{2n}\frac{e^2}{2R} \tag{8.5}$$

and

$$\alpha_n = \frac{(\varepsilon-1)\,(n+1)}{\varepsilon_2\,(\varepsilon n+n+1)} \text{ with } \varepsilon = \frac{\varepsilon_2}{\varepsilon_1}$$

$$\mathbf{P}_M\left(\mathbf{r}_1,\mathbf{r}_2\right) = \sum\nolimits_{n=0}^{\infty}\alpha_n\frac{\varepsilon_2 + r_1^n r_2^n}{R^{2n+1}}P_n\left(\cos\theta\right) \tag{8.6}$$

Here, θ is the angle between r_1 and r_2 and P_n is a Legendre polynomial.

When R is larger than $r_1$and r_2

$$V \to \frac{\varepsilon^2}{\varepsilon_2\left|r_1 - r_2\right|} \tag{8.7}$$

This is the potential energy (third) term given in Eq. (8.2) while writing the Hamiltonian term for the Mott-Wannier exciton.

We can now write the Schrödinger equation as

$$\left[-\frac{\hbar^2}{2m}\nabla_e^2 - \frac{\hbar^2}{2m}\nabla_e^2 + V_0\left(\mathbf{r}_e, \mathbf{r}_h\right)\right]\Phi\left(\mathbf{r}_e, \mathbf{r}_h\right) = E\Phi\left(\mathbf{r}_e, \mathbf{r}_h\right) \tag{8.8}$$

Consider $V_0 = \infty$ outside the sphere.

For small values of R (nanoparticles) we consider wave function $\psi_n(\mathbf{r})$ of the type

$$\psi_n\left(\mathbf{r}\right) = \frac{Cn}{\mathbf{r}}\sin\left(\frac{n\pi r}{R}\right) \tag{8.9}$$

with

$$E_n = \frac{n^2\pi^2\hbar^2}{2mR^2} \tag{8.10}$$

Here m is the effective mass of the charge (electron or hole).

Consider

$$\Phi_0 = \psi\left(\mathbf{r}_e\right)\psi\left(\mathbf{r}\right) \tag{8.11}$$

as the wave function for Eq. (8.8).

In such a case the energy of the first excited state would be

$$\Delta E = \frac{\hbar^2\pi^2}{2R^2}\left[\frac{1}{m_e} + \frac{1}{m_h}\right] - \frac{1.8e^2}{\varepsilon_2 R} + \text{polarization energy} \tag{8.12}$$

The first term on the right hand side of the equation is localization energy of electron and hole whereas the second term is due to Coulomb interaction energy between electrons and hole. The third term is due to polarization of the cluster but is usually very small and size independent, hence neglected. Details of the formulations are not given here but can be found in the original paper by L.E. Brus. The first two terms have signs opposite for each value of R. But as the particle size decreases, the first term starts dominating and ΔE starts increasing rapidly. This would effectively mean that the energy gap in a semiconductor which is characteristic of a material (e.g. CdS $E_g = 1.42$ eV, ZnS $Eg = 3.6$ eV, GaAs $Eg = 1.42$ eV) would increase with decreasing particle size or in other words we obtain size dependent energy gap which is

$$\text{Total energy} = E_{g(\text{bulk})} + \Delta E\ (\text{exciton}) \tag{8.13}$$

Obviously, ΔE becomes important when cluster size is comparable to the excitation size. This can be seen from the example given in Table 8.2, where ΔE for various values of R for GaAs are shown.

Table 8.2 Kinetic energy, Coulomb energy, energy shift ($\triangle E$) and total energy gap calculated using Eq. (8.11) for spherical particles of GaAs of various radii

	Particle radius (nm)			
Energies (eV)	20	10	5	2
Kinetic energy	0.015	0.059	0.24	1.48
Coulomb energy	−0.012	−0.024	−0.489	−0.119
Energy shift ($\triangle E$)	0.003	0.039	0.19	1.361
Total energy gap (E_g)	1.42	1.46	1.61	2.78

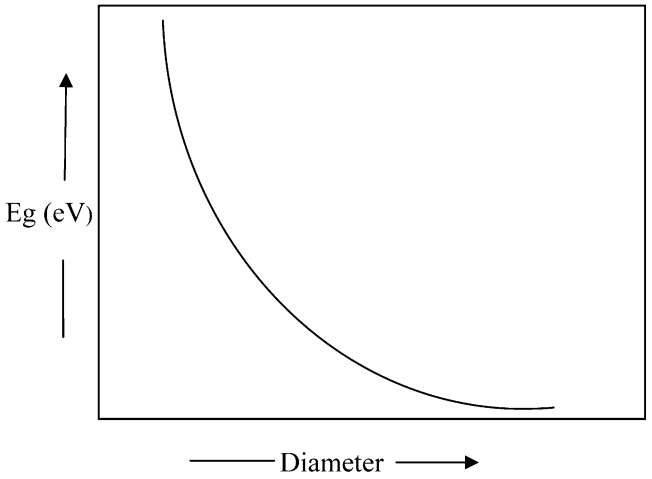

Fig. 8.6 Schematic representation of variation of energy gap with particle size

8.3.3 Optical Properties of Semiconductor Nanoparticles

The simplest experiment to determine the size dependence in semiconductor nanoparticles is to study absorption spectrum of the material as a function of wavelength of incident photons. When photons are incident on semiconductor material they will be absorbed only when the minimum energy of photons is enough to excite an electron from the valence band to conduction band, i.e. when the photon energy equals the energy gap of the semiconductor. If lower energy photons are incident, there cannot be any absorption. Therefore there is a sudden rise in absorption when the photon energy is same as the energy gap. This is the onset of absorption. If the energy gap increases there should be a shift in the onset of absorption towards the shorter wavelength. As shown in Fig. 8.6, one expects a blue shift with absorption in smaller and smaller particles, which is indicative of increasing energy gap. For every small particle (see Fig. 8.7) one often uses the terminology borrowed from chemistry, viz. Highest Occupied Molecular Orbital (HOMO) and Lowest Unoccupied Molecular Orbital (LUMO) instead of top of valence band and bottom of conduction band used in case of extended solid.

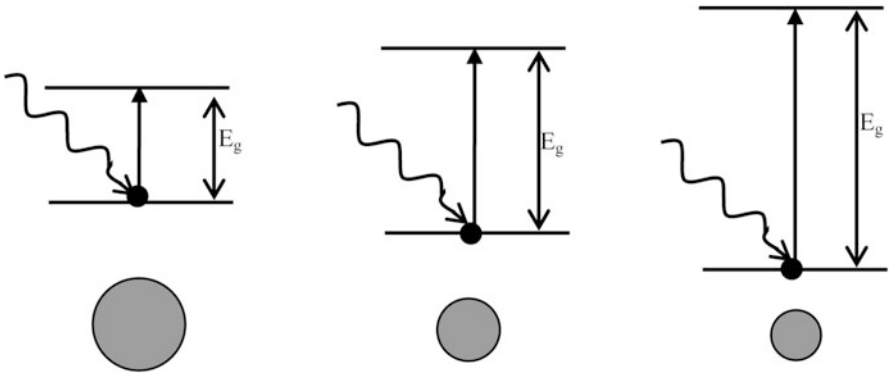

Fig. 8.7 With decreasing particle size, energy gap increases. This would give rise to blue shift in the absorption spectra

This change in absorption would have an interesting effect on the originally coloured materials. It is known now from literature that Cd_3P_2 is a dark brown semiconductor with energy gap of approximately 0.5 eV. When its particles are made, it progressively passes through a series of colours like brown, red, yellow and white with particle size changing from ∼30 to ∼15 Å. For ∼15 Å particles the band gap increases to 4 eV.

The same is true for CdS (Figure in the preface of this book). The bulk semiconductor with energy gap of 2.42 eV is orange in colour. As the particles become smaller and energy gap increases it becomes yellowish and ultimately white. It is quite easy to show by chemical analysis techniques that this white material is CdS and nothing else. In fact, observation of different colours due to CdSe in glass matrix led scientists to think that CdSe nanoparticles of different sizes might have been formed.

Many nanomaterials exhibit enhanced luminescence as compared to their bulk counterparts. Some materials like silicon which are not luminescent in their bulk form become luminescent in the nano form. Therefore luminescence investigations of nanomaterials are often carried out and are quite interesting.

We shall discuss here the principles of (a) photoluminescence, (b) electroluminescence, (c) cathodoluminescence and (d) thermoluminescence.

8.3.3.1 Photoluminescence

When the external stimulus is electromagnetic radiation or photons, the observed luminescence is known as photoluminescence. An electron from the valence band can be excited to a level in the conduction band if photon of sufficient energy to make a transition is available. This process leaves a hole in the valence band as shown in Fig. 8.8. The excited electron can loose energy by emission of phonon in a relatively shorter time ($\sim 10^{-12}$–10^{-13} s) before it can relax and make a radiative

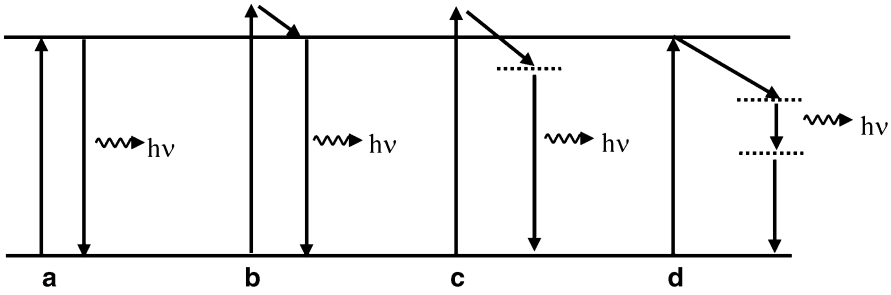

Fig. 8.8 Various processes of luminescence

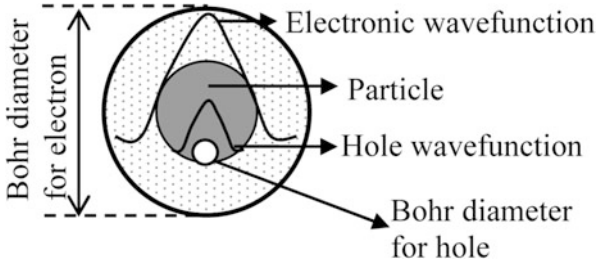

Fig. 8.9 Localization of electron and hole wavefunction inside a nanoparticle

transition (Fig. 8.8b). The life time of radiative process is much longer $\sim 10^{-7}$ to few milliseconds (fluorescence) or even few seconds (phosphorescence) than the life time of nonradiative transition.

Various possibilities of luminescence mechanisms are illustrated in Fig. 8.8. When emission of light due to the transition of an electron from the valence band maximum to the conduction band minimum, as shown in Fig. 8.8a, takes place it is called the band edge emission. The energy of emitted light or photoluminescence is the energy difference between the conduction band minimum and the valence band maximum. It is also possible as in Fig. 8.8c that the electron is first excited to the conduction band from where it moves in the material and gets trapped in some localized level. Subsequently it makes a radiative transition to valence band emitting the photon of a longer wavelength compared to that emitted by band edge luminescence. If there are localized levels introduced by impurities in the energy gap then non-radiative transition from conduction band minimum to impurity level occurs, followed by radiative transition to the lower levels (Fig. 8.8d) and then another non-radiative transition to valence band maximum.

The wavelength of luminescence, luminescence efficiency and radiative lifetime depend upon the material. In case of nanomaterials additionally the size of the material plays an important role. This can be readily understood by considering the schematics in Fig. 8.9 shown for a spherical nanoparticle.

In a particle with dimension comparable to Bohr diameter of electron, electron and hole wavefunctions can overlap. Therefore the probability of efficient recombination increases. Due to altered electronic structure in nanomaterials, the transition

rules also relax in certain cases and some transitions which are forbidden in bulk material become possible. The fluorescent efficiencies in general are found to be enhanced in nanoparticles. Interestingly, doping of nanoparticles also is possible. Dopants can introduce some energy levels in the band gap of the host material as discussed above. Such levels can be responsible for altering the luminescence properties of the host material. As an example, consider the doping of ZnS nanoparticles with manganese. ZnS is a wide direct band gap material. The band gap luminescence of bulk ZnS is at ~344 nm. If Mn is introduced in small quantity (~0.1 at. %) it produces discrete energy levels in the band gap. A photoexcited electron can make a transition from conduction band minimum to upper level and then combine with a trapped hole in lower level to emit luminescence at ~590 nm. In nanoparticles also such luminescence is observable but with more probability or higher luminescence efficiency, due to increased overlap, arising because of small size in nanoparticles, of wavefunctions. The process can be accompanied by band edge luminescence and/or defect emission.

8.3.3.2 Electroluminescence

Luminescence observed by the application of an electric field to a material is known as electroluminescence. It can be observed by applying either low or high ($>10^4$ V/cm) field; accordingly it is classified as 'injection luminescence' and 'high field electroluminescence' respectively.

Injection luminescence: Light emitting diodes are based on the principle of minority carrier injection in a diode. When a p-n diode is formed, a depletion region is set up with V_d as the diffusion potential between the p-n regions (see Fig. 8.10).

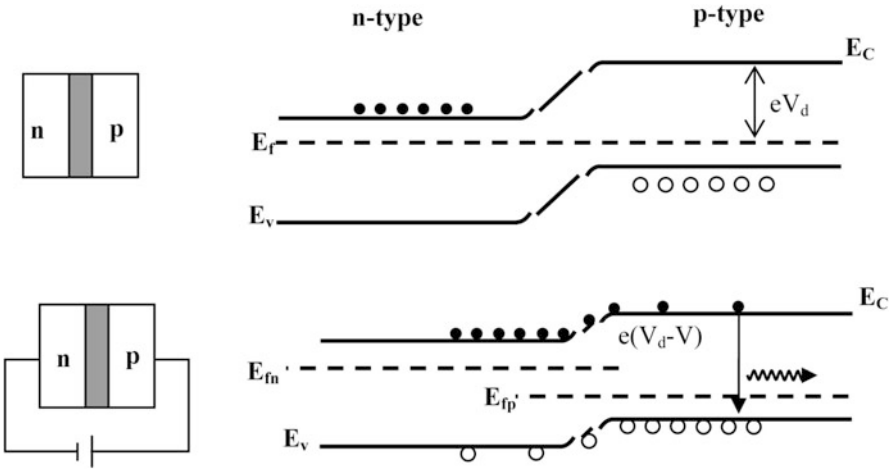

Fig. 8.10 p-n junction at thermal equilibrium (*upper*) and with forward bias

In a p-type semiconductor, holes are the majority carriers and electrons are minority carriers. On the other hand, in an n-type semiconductor, electrons are majority carriers and holes constitute minority carriers.

By forward biasing the diode, the diffusion barrier can be reduced and potential becomes V_d–V, where V is the applied voltage. Under this condition, the electrons from n-region find it easier to travel to p-region and holes can easily migrate from p-region to n-region. Thus minority carriers are injected on each side. The injected carriers can combine with easily available opposite charge carriers in each region to produce luminescence.

It can be observed that the injection luminescence is a 'band edge' type luminescence. Therefore for a fixed semiconductor, the wavelength of luminescence is fixed. However in nanomaterials we know that energy gap can be tuned with particle size. Hence the luminescence also can be tuned to desired wavelength in nanomaterials.

High field electroluminescence: This type of electroluminescence is used in 'display panels'. Emission of electrons by application of very high electric field ($\sim 10^5$–10^7 V/cm) is known as *field emission*. As illustrated in Fig. 8.11 an energy barrier existing for a material has to be overcome by an electron in order to leave it. The barrier, however, reduces on application of the electric field, the width of which depends on the applied field. As can be seen from the figure, more the applied field, smaller is the width of the barrier. In general, an electron needs energy sufficient to overcome the barrier in general. However quantum mechanically, if the barrier width is reduced sufficiently, the electrons can tunnel through the barrier. This type of field emission requires very high field as mentioned above.

In a metal semiconductor contact, the barrier height is reduced due to transfer of electrons either from metal to semiconductor or semiconductor to metal depending upon the type (n or p) and value of work functions of both metal and semiconductor. A metal-semiconductor contact is known as Schottky barrier. Electrons can be

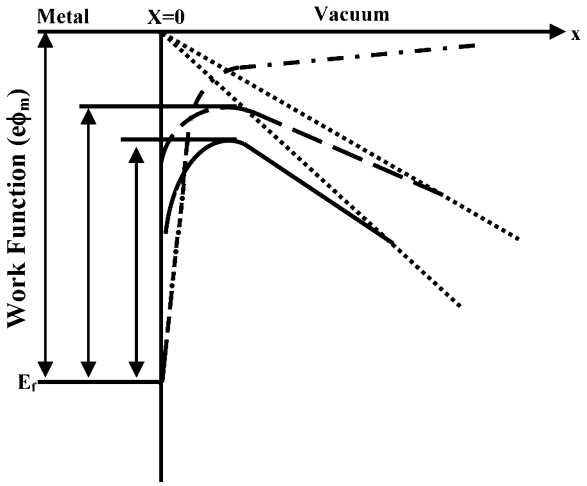

Fig. 8.11 Field emission from a metal

injected from metal to p-type semiconductor by high electric field. Note that here electrons are emitted from metal into the semiconductor by a different phenomenon as compared to that in injection luminescence. In injection luminescence, charge carriers overcome the potential barrier and penetrate the other material whereas in high field luminescence it is through tunneling as the electrons pass from metal to semiconductor. After passing from metal to semiconductor, if the electron comes in the vicinity of a hole it combines radiatively.

High field luminescence in nanomaterials: Nanomaterials are useful in display panels using high field. The fine particles resolve the images better as compared to microparticles. However due to high quantum efficiency of luminescence, electroluminescence also is an efficient process.

8.3.3.3 Cathodoluminescence

Electrons of very high energy striking a semiconductor material produce luminescence known as 'cathodoluminescence'. The incident electrons here are from some filament or field emission cathode. They strike the luminescent material in vacuum at high energy. The electrons on impact with the material are able to loose their energy by various processes. Phenomenon of cathodoluminescence is used in oscilloscope and old television display screens.

Nanomaterials are also useful to produce high efficiency cathodoluminescence due to the same reasons as for high field luminescent materials. Cathodoluminescence in ZnS doped with Mn and ZnO nanoparticles has been investigated. It has been observed that nanoparticles are better luminescent materials than microparticles of the respective material.

8.3.3.4 Thermoluminescence

In semiconductors with large band gaps it is found that if they are excited at very low temperatures with photons in the UV range, on heating to some temperature which depends upon the dopant ions, light is emitted even in the absence of any other stimulus. The phenomenon is known as 'thermoluminescence' or 'after glow'.

As illustrated in Fig. 8.12, luminescence is due to trapped electrons. The trapped electrons are activated by thermal energy and can combine with hole making radiative transition or causing luminescence. Figure 8.12 also gives some examples in which luminescence due to different co-activation is observed for ZnS doped with Cu. Observation of thermoluminescence is an effective method of studying the trap levels in materials.

Nanomaterials also have defect levels. The surface atoms can act as efficient traps for electrons/holes. Therefore thermoluminescence can be quite strong in nanomaterials. Thermoluminescence has been reported for ZnS nanoparticles doped with copper and other co-dopants (or co-activators) illustrated in Fig. 8.12.

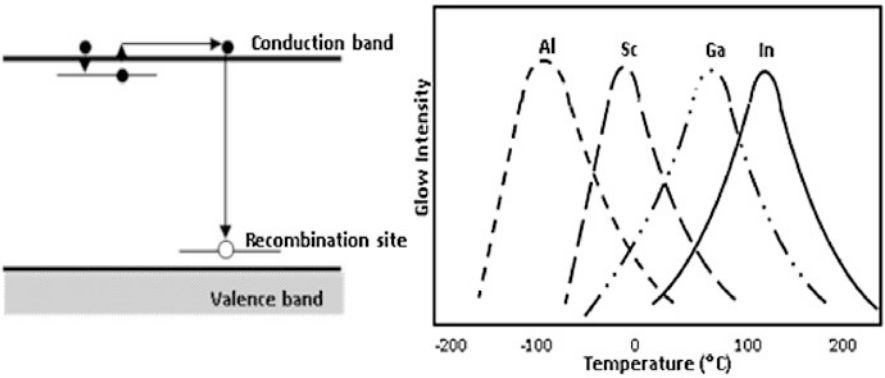

Fig. 8.12 Thermoluminescence energy level diagram

8.4 Plasmonic Materials

Windows in old churches, palaces, houses etc. are designed with beautiful tinted glasses. Such glasses are made by dissolving small amount (<5 %) of metal particles like gold, silver, cobalt, iron and nickel. Such glasses are transparent but have different colours like red, pink, blue, green or other shades depending upon the dissolved metal particles. Indeed the colour of glasses is due to metal nanoparticles. Note that the colours produced by dissolving the metal powders are not same as their bulk metal colour. For example gold metal has yellow 'golden' colour in the bulk form but the colour produced by dissolving small amount of gold in glass may be reddish, pink or even blue. Although the art of making tinted glasses is more than 2,000 years old, scientific interest in metal nanoparticles started with M. Faraday's synthesis of gold nanoparticles in 1857. He reduced chloroauric acid ($HAuCl_4$) using citric acid [$CH_2(COO)_2H_2O$] and showed that Au metal nanoparticles produced intense magenta-red colour as against yellow appearance of bulk gold metal. Attempts were since then made to explain the observed intense colours due to metal nanoparticles. Apart from their beautiful appearance, it is now realized that metal nanoparticles have applications in sensors, solar cells, cancer therapy, cloaking devices and photonic devices for communication or optical circuits. Here we will try to understand the theories developed to explain the observed behaviour of metal nanostructures. It should be remembered that metal nanoparticles differ from the semiconductor particles. Metals have a large free electron density of valence electrons $\sim 10^{22}$–$10^{23}/cm^3$. On the other hand semiconductors have much lower electron density $\sim 10^{16}$–$10^{18}/cm^3$ depending upon the level of doping. Doping is a process of introducing electron donor or acceptor atoms in small quantities in order to make the n or p type semiconductors. Therefore in semiconductor nanomaterials the observed properties are explained based on the electron confinement in a potential well of appropriate shape depending on the nanomaterial dimensionality (0-D, 1-D or 2-D). In metal nanostructures a

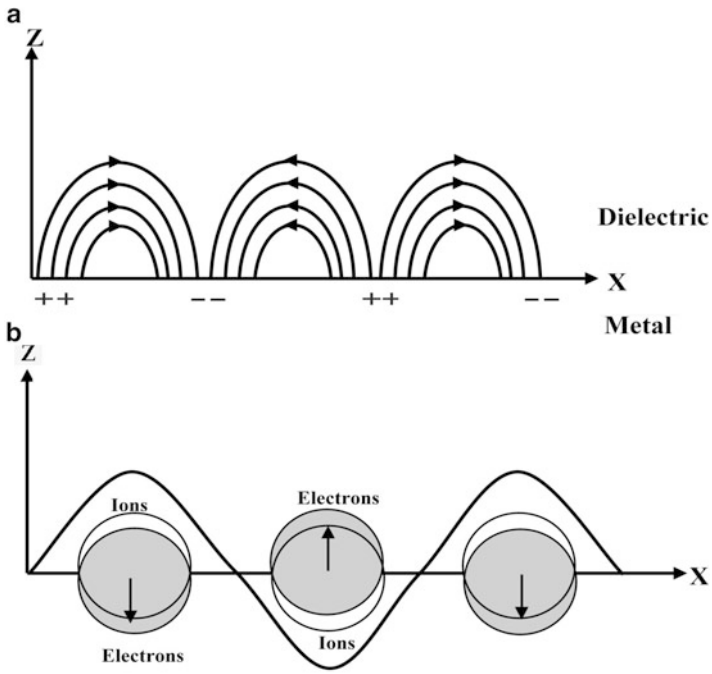

Fig. 8.13 Schematic of SPR: (**a**) Propagating SPR and (**b**) Localized SPR

large number of electrons are considered together and the confinement is often known as 'dielectric confinement' rather than 'electron confinement'. We now proceed to discuss how to describe observed behaviour of metal nanoparticles and nanostructures.

The small particles of different shapes like spherical particles, wires, rods, cubes and thin films or surfaces of metals need to be treated differently. The small particles exhibit *localized surface plasmon resonance* (SPR) and surfaces of metals or thin films have propagating surface waves viz. *surface plasmon polariton* as separately discussed below and schematically illustrated in Fig. 8.13.

8.4.1 Localized Surface Plasmon Resonance

In 1908, G. Mie explained by using Maxwell's equations the scattering (and absorption) of light from very small particles. When electromagnetic radiation is incident on the spherical particles of uniform size, embedded in a medium, reduction in intensity is observed. It is necessary to consider mainly the dielectric constant of medium in which the particles float and the dielectric constant of the particles. Interaction between the particles is neglected in Mie theory (Fig. 8.14). His theory can be briefly described as follows. The details can be found in some standard text books on optics.

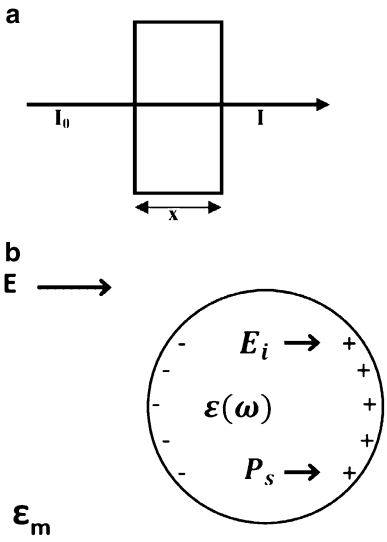

Fig. 8.14 (**a**) Incident radiation I_0 passes through a medium of thickness x and (**b**) A particle embedded in a dielectric medium (Mie theory)

A beam of electromagnetic radiation of intensity I_0 and wavelength λ passes through a medium having dielectric constant ε_m. If the particles are embedded uniformly in the medium and multiple reflections do not take place, the transmitted intensity would be given by D'Lambert equation

$$I = I_0 e^{-\mu x} \tag{8.14}$$

where μ is extinction coefficient.

$$\mu = \frac{N}{VC_{ext}} \tag{8.15}$$

N is the number of particles in medium, V – the volume of colloidal particles and C_{ext} is extinction cross section of a particle.

$$C_{\text{ext}} = C_{\text{abs}} + C_{\text{scatt}} \tag{8.16}$$

In the Mie theory

$$C_{\text{ext}} = \frac{2\pi}{k^2} \sum_{n=1}^{\infty} (2n+1)\, R_e\, (a_n + b_n) \tag{8.17}$$

where a_n and b_n are scattering coefficients. They are functions of a and λ in terms of Ricatti-Bessel functions. The details of the Mie theory can be found in the book by Born and Wolf (see the complete reference at the end of this chapter).

$$k = \frac{2\pi\sqrt{\varepsilon_m}}{\lambda} \tag{8.18}$$

For very small particles ($kR \ll 1$) having radius R, extinction is mainly due to absorption. The extinction coefficient is given by

$$C_{\text{ext}} = \frac{24\pi^2 \mathrm{R}^3 \varepsilon_m{}^{\frac{3}{2}}}{\lambda} \frac{\varepsilon_2}{(\varepsilon_1 + 2\varepsilon_m)^2 + \varepsilon_2^2} \tag{8.19}$$

where

$$\varepsilon(\omega) = \varepsilon_1(\omega) + i\,\varepsilon_2(\omega) \tag{8.20}$$

$\varepsilon(\omega)$ is the dielectric constant of the particles. As can be seen from above equation, C_{ext} depends on R^3. Absorption coefficient μ is inversely proportional to $1/V$ i.e. $1/R^3$. Thus absorption is independent of particle size. From the equation (8.19), it is also seen that extinction would be maximum when

$$\varepsilon_1 + 2\varepsilon_{\text{m}} = 0 \text{ or } \varepsilon_1 = -2\varepsilon_{\text{m}} \tag{8.21}$$

if ε_2 is small. This gives rise to strong resonance band. Bandwidth and peak height is mainly determined by $\varepsilon_2(\omega)$ (interestingly C_{ext} vanishes if $\varepsilon_2 = \infty$ as well as $\varepsilon_2 = 0$).

Although Mie theory successfully explains the observation of an absorption band for metal nanoparticles in the visible range of wavelengths, for particle size less than ~10 nm, it hardly explains the observed shifts in the absorption peaks with change in the particle size. One, therefore, should consider dielectric constant which depends not only on the wavelength (or frequency) but also on the particle size. For metals the dielectric response of electrons is better described by Drude model. The theory of LSPR is based on the Drude model of dielectric response of free electrons in a metal. Consider that the electric field vector of an electromagnetic wave with frequency ω is written as

$$E = E_0 \exp(-i\,\omega t) \tag{8.22}$$

on a metal particle. The electrons of mass m are then accelerated. The equation of motion is given as

$$m\frac{d^2x}{dt^2} + \gamma\frac{dx}{dt} + m\omega_0^2 x = eEe^{-i\,\omega t} \tag{8.23}$$

An electron in a metal experiences collisions (which give rise to resistivity in materials) with lattice and impurities. The relaxation time of an electron is $\tau = 1/\gamma$. Solving the Eq. (8.23) we get

$$x = \frac{eE/m}{\omega_0^2 - \omega^2 - i\,\omega_d\,\omega} \tag{8.24}$$

where $\omega_0{}^2 = f/m$, in which 'f' is the restoring force constant, and $\omega_d = \gamma/m$ is the damping. The resonance frequency here is ω_0 and it may or may not be equal to the frequency of the incident radiation.

The electron displacement 'x' is in the same direction of applied field when the resonance frequency ω_0 is more than the incident frequency ω. The displacement can be negative if $\omega > \omega_0$.

Consider that the displacement x is not just for a single electron but for N electrons/cm^3 in a particle, then they would create polarization **P**

$$\mathbf{P} = N\, e\mathbf{x} \tag{8.25}$$

Polarization can also be written in terms of the dielectric function as

$$\mathbf{P} = \varepsilon_0 (1 - \varepsilon)\, \mathbf{E} \tag{8.26}$$

Using the equations

$$\varepsilon(\omega) = 1 + \frac{Ne^2/m\varepsilon_0}{\omega_0^2 - \omega^2 - i\omega_d\omega} \tag{8.27}$$

and

$$\varepsilon(\omega) = \varepsilon'(\omega) + i\varepsilon''(\omega) \tag{8.28}$$

where ε' and ε'' are the real and imaginary parts of the dielectric functions respectively. Therefore,

$$\varepsilon'(\omega) = 1 + \frac{\left(\omega_0^2 - \omega^2\right)\omega_p^2}{\left(\omega_0^2 - \omega^2\right)^2 + \omega^2\omega_d^2} \tag{8.29}$$

When $\omega_0 = 0$ and $\varepsilon(\infty) = 1$, $\omega_p^2 = \dfrac{4\pi Ne^2}{m}$ is the volume plasma, (8.30)

$$\varepsilon'(\omega) = \varepsilon(\infty) - \frac{\omega_p^2}{\omega^2 + \omega_d^2} \tag{8.31}$$

and

$$\varepsilon''(\omega) = -\frac{\omega_d\omega_p^2}{\omega\left(\omega^2 + \omega_d^2\right)} \tag{8.32}$$

$\omega_0 = 0$ is possible when the electrons do not have any restoring force. $\varepsilon(\infty)$ is the dielectric constant at very high frequency.

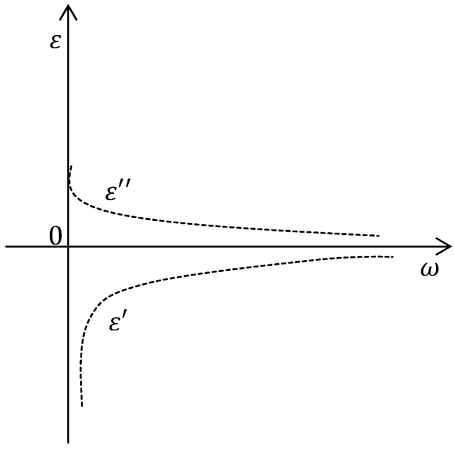

Fig. 8.15 Real and imaginary parts of the dielectric function with respect to the frequency

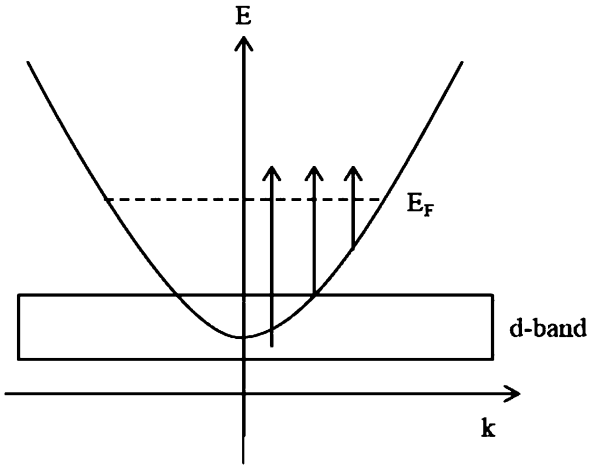

Fig. 8.16 Schematic diagram of various transitions from filled inter and intra bands in a metal

When $\omega_0 = 0$, the electrons are out of phase with the electric field **E**. This implies that the real part of the dielectric constant would always be negative. This is schematically shown in Fig. 8.15.

Additionally, as shown schematically in Fig. 8.16, the electrons from the conduction band (*s*) and the filled band (*d*) to empty states above the conduction band also get photo-excited.

Thus the dielectric constant may get further modified by interband transitions. In silver and gold, the real part of the dielectric constant gets modified due to contribution from the 'd' and 'sp' bands. In the visible and ultra-violet regions, interband transitions contribute substantially whereas the 'red' or the long wavelengths derive contributions from intraband transitions.

Further, one needs to take into account that at small sizes of metal particles, the collisions of electrons with surface of the particle would increase. Therefore, the damping term γ would become

$$\gamma = \gamma_0 + g\frac{v_{F0}}{D} \tag{8.33}$$

where g is a proportionality factor ($\sim$1), v_F – the velocity of electrons at the Fermi surface, and D is the diameter of the particle. If D is much smaller than the wavelength of incident radiation and the resonance condition given by $\varepsilon' + 2\varepsilon_m = 0$, is satisfied, the resonance will occur at

$$\Omega(r) = \frac{\omega_p}{\sqrt{\varepsilon'_{\text{interband}} + 2\varepsilon_m}} \tag{8.34}$$

One can see from the above equation and the discussion in this section, how the dielectric constant of the metal particles (alongwith the dielectric constant of the medium in which they are dispersed) determines the position of the SPR peak. Therefore the phenomenon of SPR is aptly referred to as the 'dielectric confinement'. This equation works well for silver, but complications arise for gold and copper due to the overlap of interband transitions with the surface plasmon band. Thus in order to explain the observed difference in the surface plasmon resonance positions of gold and silver nanoparticles in spite of almost same lattice constants and electron density (hence ω_p which is 8.98 eV for silver and 9.01 eV for gold), it is necessary to remember that interband transitions need to be taken into account. In Table 8.3 values for some metals in vacuum ($\varepsilon_m = 1$) are given.

For the silver nanoparticles, surface plasmon resonance peaks are much sharper compared to those due to gold nanoparticles. This is due to the occurrence of silver plasmon resonance peak where imaginary part of dielectric constant (ε'') has nearly zero value. This is not the case for gold, for which absorption due to interband transition for ε'' has finite value.

Interestingly only few metals like gold, silver, copper and palladium nanoparticles show surface plasmon resonance in the visible range or close to visible range. There are many metals which surprisingly do not exhibit strong resonance peaks in the visible range. This is because they have interband transitions spread over UV-VIS-IR region which overlap with their resonance energies making them difficult to observe.

Table 8.3 Values for some metals: $\hbar\Omega$(ib) – interband energy and $\hbar\Omega$(r) – surface plasmon energy

	m_e (effective mass of electron)	N (e/m^3)	1 (nm)	v_F (10^6 m/s)	ω_p (eV)	$\hbar\Omega$(ib) (eV)	$\hbar\Omega$(r) (eV)
Ag	1.03	5.85	55	1.4	8.98	3.9	3.5
Au	1.01	5.9	42	1.4	9.01	2.3	2.4
Cu	1.17	8.48	28	1.05	9.05	2.1	2.0

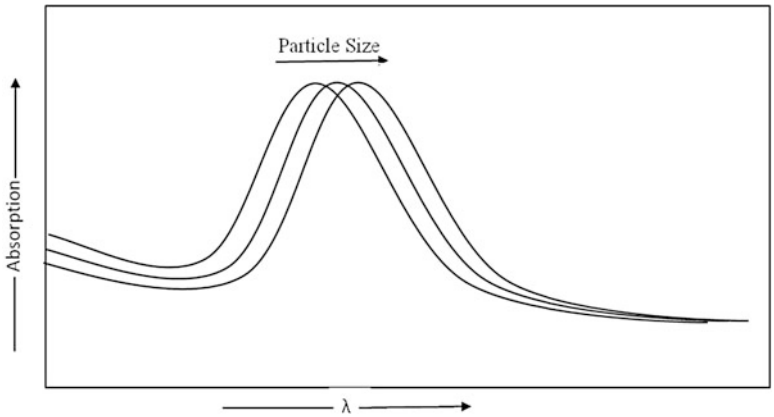

Fig. 8.17 The surface plasmon resonance absorption peak position red-shifts with increase of the particle size

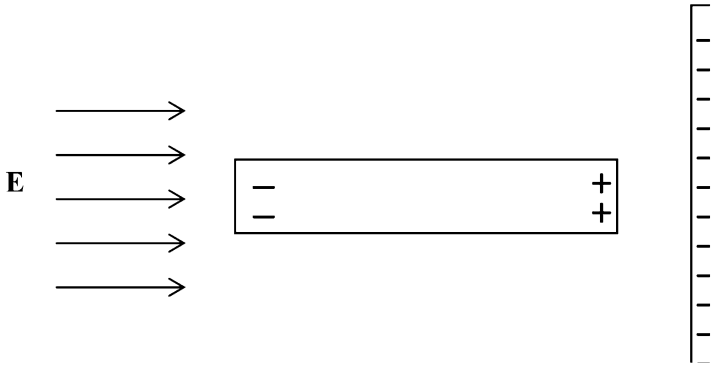

Fig. 8.18 Illustration of the change in the magnitude of the polarization due to the orientation of nanorods

For a given metal nanoparticle surface plasmon resonance energy is affected by the medium (dielectric constant) in which they are embedded. The surface plasmon resonance peak position also depends on the particle size (Fig. 8.17).

Usually small particles are dominated by absorption and large particles by scattering. Gold and silver nanoparticles also show effects on surface plasmon resonance due to shape. This is easily attributed to the differences in their polarization/depolarization effects. The orientation of nanoparticles with respect to the incident radiation also would get modified (see Fig. 8.18). For example a nanorod standing parallel or transverse to the incident beam would have different value of C_{ext}.

A nanorod also readily shows two surface plasmon resonance peaks as shown in Fig. 8.19.

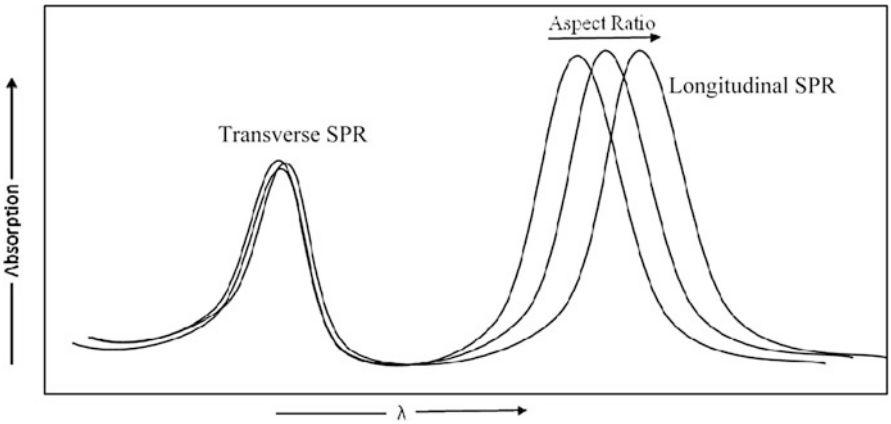

Fig. 8.19 Transverse and longitudinal surface plasmon peaks of nanorods. With increasing rod length the longitudinal plasmon resonance peak keeps on shifting to the longer wavelength but transverse resonance peak remains at the same position if the diameter of the rod remains unchanged

The two peaks appear due to the cross section (diameter) and length of the particle. If the diameter of the nanorod is kept constant and length changed, it is also possible to keep the resonance peak due to cross section at same energy and vary the longitudinal peak (due to length). The length/diameter or aspect ratio variation is often made in order to meet the needs of some applications.

Numerous other shapes like cubes, stars, tetra pods, flowers and so on are observed by tuning the synthetic conditions. They produce tunable surface plasmon resonance peaks.

Temperature is another parameter which can affect the surface plasmon resonance. With increase in temperature, volume expansion takes place shifting the electron density. This causes a red shift in the resonance peak position. The peak broadening also can occur as a result of increased scattering of electrons. The solvent temperature decreases its refractive index which shifts the resonance peak to blue side.

8.4.2 Surface Plasmon Polariton

Surface plasmon polaritons have become very important in nanotechnology because the scientists are quite hopeful of developing a branch called *nanophotonics* using them. Using some metallic nanostructures or thin films, unlike in localized surface plasmon resonance, it is possible to let the waves of surface plasmon polaritons to propagate along the interface between metal surface and a dielectric (vacuum, air, glass or any other dielectric medium) medium over large distances. This is because of the coupling of the electromagnetic radiation and the surface plasmons.

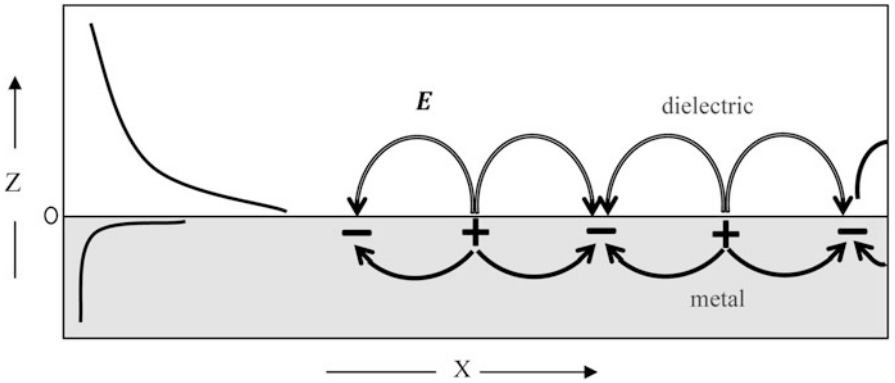

Fig. 8.20 Surface plasmon polariton. Metal shown in *grey* and *white* portion of the figure is dielectric

Coupling of a photon and surface plasmon is known as *surface plasmon polariton*. It should be remembered that polariton is a general term used to refer to any coupling between a photon and an elementary excitation (exciton, phonon and plasmon). Thus surface plasmon polaritons are confined and can travel over large distances of even few micrometres which makes them very useful to transfer the light from one end to the other end of the nanostructure. This becomes useful to design nano optical devices and circuits.

As shown in Fig. 8.20, there are two components of the surface plasmon polariton viz. longitudinal (along X-axis) and the transverse (along Z-axis).

The electric field inside the metal can be written as

$$E_{\mathrm{m}}(x,z,t) = E_{\mathrm{m},0}\, e^{i(k_x x - k_z z - \omega t)} \tag{8.35}$$

and in the dielectric as

$$E_{\mathrm{d}}(x,z,t) = E_{\mathrm{m},0}\, e^{i(k_x x - k_z z - \omega t)} \tag{8.36}$$

Note that *m* and *d* denote metal and dielectric. The electric field has both x and z components, although the amplitudes decay exponentially inside the metal as well as dielectric medium as shown on the left side of Fig. 8.20. Using the Maxwell's equations the dispersion relation can be shown as

$$k_{\mathrm{x}} = \frac{\omega}{c}\left(\frac{\varepsilon_{\mathrm{m}}\varepsilon_{\mathrm{d}}}{\varepsilon_{\mathrm{m}} + \varepsilon_{\mathrm{d}}}\right)^{1/2} \tag{8.37}$$

with

$$k_{\mathrm{x}} = \frac{\omega}{c}\sqrt{\varepsilon}$$

ε_{m} and ε_{d} are dielectric constants of the metal and dielectric respectively.

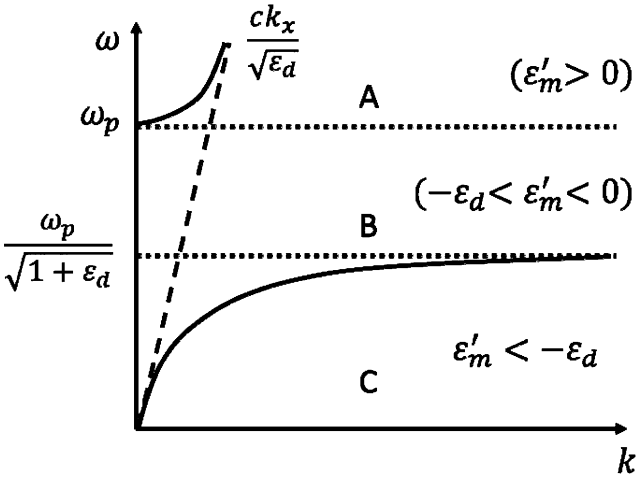

Fig. 8.21 Dispersion curve for the surface plasmon polariton

The dispersion behaviour of surface plasmon polariton can be understood from Fig. 8.21.

The dotted line represents the dispersion of light in the dielectric medium, air with $\varepsilon_d = 1$ here. Obviously the dispersion is divided into three parts, A, B and C, depending upon the dielectric constant values of the metal. Here we consider the real part of the dielectric constant viz. ε'.

When $\omega > \omega_p$ (region A),

$$\varepsilon_m \text{ and } \varepsilon_m + \varepsilon_d \text{ are } > 0 \tag{8.38}$$

The modes are radiative. In this region, k_x and k_z are both real.

In the region B, we have

$$\frac{\omega_p}{\sqrt{1+\varepsilon_d}} < \omega < \omega_p \tag{8.39}$$

Here $\varepsilon_m < 0$ but $\varepsilon_m + \varepsilon_d > 0$ and k_x is imaginary but k_z is real and no propagating modes exist.

In the region C,

$$0 < \omega < \frac{\omega_p}{\sqrt{1+\varepsilon_d}} \tag{8.40}$$

The quantities ε_m and $\varepsilon_m + \varepsilon_d$ are < 0 and k_x is real but k_z is imaginary. When the values of k_x are small they approach the dotted line for dispersion of light in the dielectric.

In region C, we have bound modes and through the coupling of the electromagnetic waves and surface plasmons, surface plasmon polaritons can be propagated along the surface without radiative decay. This is what is expected in this branch of nanophotonics.

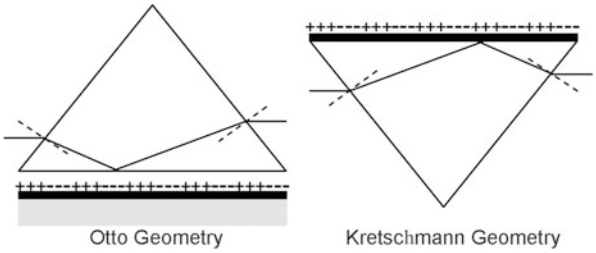

Fig. 8.22 The light rays passing through the prisms couple with the surface plasmons shown as positive–negative charge waves on the metal thin film (*dark black*). By keeping the analyte between the prism and the metal thin film, either in Otto or Kretschmann geometries, analytes can be studied by finding out the changes in the reflected rays

We shall not go into more details about surface plasmon polaritons here but just mention that surface plasmon modes and electromagnetic modes can be coupled also at the glass prism/dielectric and metal surface as illustrated in Fig. 8.22. Two different configurations can be set to investigate the surface plasmon polariton or to make its application as a sensor.

The light rays are internally reflected at glass prism and a dielectric between metal thin film, known as Otto configuration as in the left of Fig. 8.22 or by depositing the thin metal film directly on the prism. The silver or gold films are often used.

8.5 Nanomagnetism

Magnetism in bulk materials is due to magnetic moments on constituting atoms, ions or molecules. Presence of a magnetic field around a moving charge is well known. In an atom, spin and orbital motion of electrons and change of orbital motion in the presence of external applied magnetic field **H**, gives rise to magnetic moment. Nuclear magnetic moment is usually very small and will be neglected in our discussion.

Total spin angular momentum due to spin of electrons in incomplete shells is given by

$$\mathbf{S} = \sum_{i}^{N} \mathbf{S}_{\mathrm{i}} \tag{8.41}$$

Where $\mathbf{S}_{\mathrm{i}}$ is the spin on the *i*th shell and the sum is over N shells. Corresponding dipole moment is given by

$$\boldsymbol{\mu}_{\mathrm{s}} = -\frac{e}{m}\mathbf{S} \tag{8.42}$$

Total orbital angular momentum due to that of electrons in incomplete shells is given by

$$\mathbf{L} = \sum_{i}^{N} \mathbf{L}_i \tag{8.43}$$

Where $\mathbf{L}_\mathrm{i}$ is the orbital momentum of *i*th shell and the sum is over all the *N* shells. The magnetic orbital angular momentum is given by

$$\boldsymbol{\mu}_\mathrm{L} = \frac{e}{2m}\mathbf{L} \tag{8.44}$$

Total angular momentum **J** is

$$\mathbf{J} = \mathbf{L} + \mathbf{S} \tag{8.45}$$

Interaction between **L** and **S** is known as spin-orbit interaction. The total magnetic moment of an atom is given by

$$\boldsymbol{\mu} = \boldsymbol{\mu}_\mathrm{L} + \boldsymbol{\mu}_\mathrm{S} \tag{8.46}$$

It can be shown (see Fig. 8.23) that in free space magnetic moment on an atom is given by

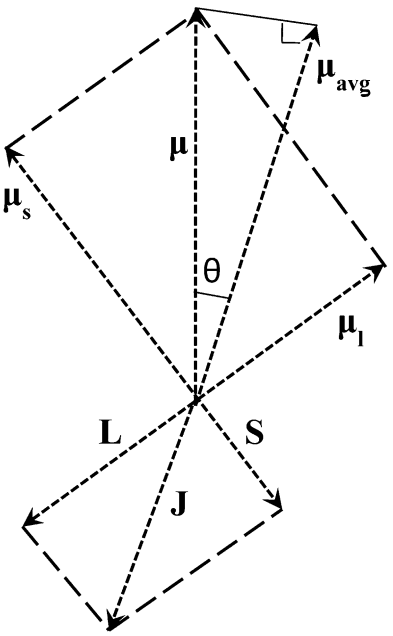

Fig. 8.23 Spin-orbit interaction

$$\boldsymbol{\mu}_{\text{avg}} = g\left(-\frac{e}{2m}\right)\mathbf{J} \tag{8.47}$$

with

$$g = 1 + \frac{\mathrm{J}(\mathrm{J}+1) + \mathrm{S}(\mathrm{S}+1) - \mathrm{L}(\mathrm{L}+1)}{2\mathrm{J}(\mathrm{J}+1)} \tag{8.48}$$

In the presence of an applied magnetic field, angular momentum can have $2\,\mathrm{J}+1$ orientations. One can determine S, L and J values if one knows the angular momentum of incomplete shells and number of electrons using Hund's rules as follows.

Hund's Rules

1. The maximum allowed value of S will be decided by Pauli's exclusion principle.
2. The maximum value of L is consistent with the value of S from L.
3. The value of J will be $|\mathrm{L}-\mathrm{S}|$ when the shell is less than half filled and $|\mathrm{L}+\mathrm{S}|$ when the shell is more than half filled.

The resultant magnetic moment of an atom could be defined as:

$$|\boldsymbol{\mu}| = \mu_{\mathrm{B}}\, g\, (\mathrm{J}(\mathrm{J}+1))^{1/2} \tag{8.49}$$

where μ_{B} is the Bohr magneton (9.3×10^{-24} Jm^2/Wb) and g is Lánde factor having a value between 1 and 2.

8.5.1 Types of Magnetic Materials

Depending upon the response of a material to the external magnetic field, i.e. how much magnetization (M) is induced in the material by an external magnetic field most of the materials can be classified as diamagnetic, paramagnetic, ferromagnetic, antiferromagnetic and ferrimagnetic. The ratio of M to H is called the susceptibility:

$$\chi = \frac{M}{H} \tag{8.50}$$

$$\mu_0 = \frac{B}{H} \tag{8.51}$$

where B is magnetic induction and μ_0 is the permeability of the free space.

Permeability of the medium μ_m is given by

$$\mu = 1 + 4\pi\chi \tag{8.52}$$

We shall now discuss these materials in brief.

8.5.1.1 Diamagnetic Materials

Diamagnetism can be considered as the atomic manifestation of Lenz's law. When a magnetic field is applied to a conducting loop, a current is induced which opposes the change of flux. Electrons in atom are equivalent to conducting loop. In the applied magnetic field, electrons precess about the magnetic field direction. The precession is known as Larmor precession. It induces a magnetic moment

$$\mu = -\left(\frac{\mu_0 e^2}{4m}\right) r^2 \mathrm{H} \tag{8.53}$$

where r is the radius of the electron orbit. There is no diamagnetic component of magnetic moment in the absence of an external magnetic field. However, as soon as an external magnetic field is present, diamagnetic component would always be present.

The magnetic susceptibility for N atoms having atomic number Z is given by

$$\chi = -\left(\frac{N\mu_0 e^2 Z}{6m}\right) a^2 \tag{8.54}$$

where a is the average radius of electrons in an atom.

Thus diamagnetic materials have temperature independent negative susceptibility.

8.5.1.2 Paramagnetic Materials

Materials having some net magnetic moment present on atoms, molecules or ions even in the zero magnetic field are paramagnetic. In the zero magnetic field these magnetic moments would be randomly distributed and the material can show zero magnetization. In the presence of the magnetic field the magnetic moments try to align themselves in the direction of the magnetic field. Thermal energy kT tries to disturb this alignment. Diamagnetic component also arises in the opposite direction of the magnetic field but paramagnetic response can be larger resulting into a net positive response. Magnetic susceptibility is given by

$$\chi = \frac{Np^2\mu_B^2 Z}{3kT} = \frac{C}{T} \tag{8.55}$$

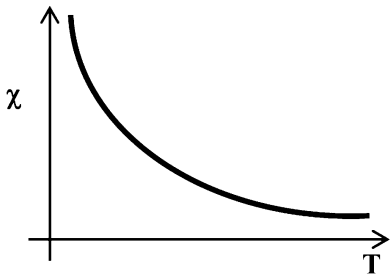

Fig. 8.24 Temperature variation of magnetic susceptibility in case of paramagnetic materials

where C is known as Curie constant and

$$p = g[J\,(J+1)]^{1/2} \tag{8.56}$$

p is known as effective Bohr magneton.

Equation (8.55) is known as Curie law. It shows that the magnetic susceptibility in case of paramagnetic substances is inversely proportional to the temperature. Figure 8.24 illustrates schematically the temperature dependence of paramagnetic susceptibility.

8.5.1.3 Ferromagnetic Materials

Some magnetic materials have regions or domains in which large number of atoms or ions or molecules having permanent magnetic moments, like in paramagnetic materials, are aligned in a particular direction. Different domains are separated by what is known as domain walls. The domains themselves may be randomly oriented in the absence of a magnetic field. Such materials are said to have spontaneous magnetization and are known as ferromagnetic materials. This is due to the magnetic interaction, known as exchange field, amongst the magnetic moments of atoms. It was proposed by Weiss that the effect of mean magnetic field due to all other moments on a given moment of an atom is given by

$$\mathbf{H} = \lambda \mathbf{M} \tag{8.57}$$

$$\mathbf{H}_{\text{total}} = \mathbf{H} + \lambda \mathbf{M} \tag{8.58}$$

Modified Curie law, known as Curie–Weiss law for the susceptibility of ferromagnetic materials, is given by the equation

$$\chi = \frac{C}{(T - T_{\text{c}})} \tag{8.59}$$

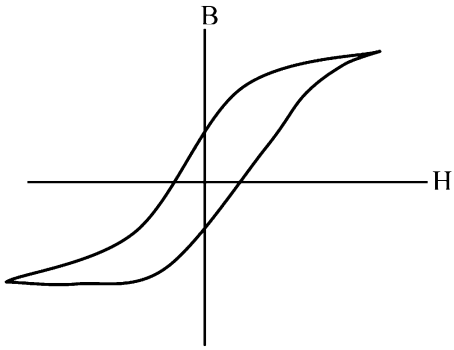

Fig. 8.25 Hysterisis loop of a ferromagnetic material

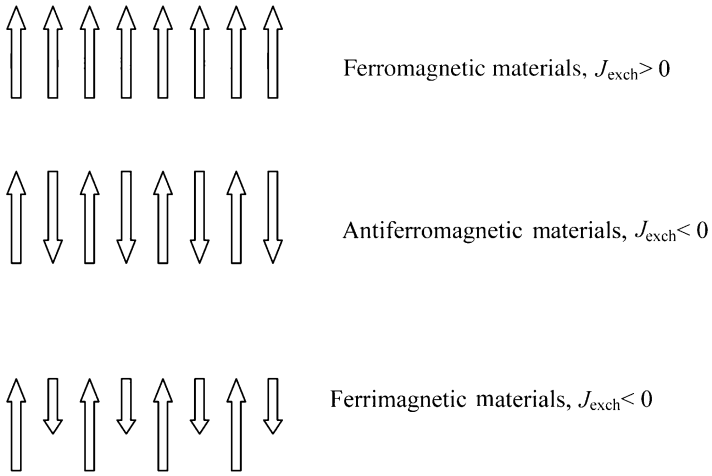

Fig. 8.26 Schematic of spin orientations on neighbouring atoms in case of ferromagnetic, antiferromagnetic and ferrimagnetic materials

where T_c is the Curie temperature. In ferromagnetic materials below the characteristic temperature T_c of the material, spontaneous magnetization exists in zero magnetic field. At temperature higher than T_c, the material behaves like a paramagnetic material. Ferromagnetic materials exhibit a hysteresis behaviour (see Fig. 8.25) of magnetization when an external magnetic field is applied.

Heisenberg explained the spontaneous magnetization by considering that the exchange energy U_{exch} which is due to the spin moments say $\mathbf{S}_i$ and $\mathbf{S}_j$ on *i*th and *j*th atoms is given by

$$U_{exch} = -2J_{exch}\, \mathbf{S}_i \cdot \mathbf{S}_j \tag{8.60}$$

where J_{exch} is known as the exchange integral.

When J_{exch} is negative, antiparallel configuration of spins is favoured, whereas for positive J_{exch}, parallel configuration is favoured, as illustrated in Fig. 8.26.

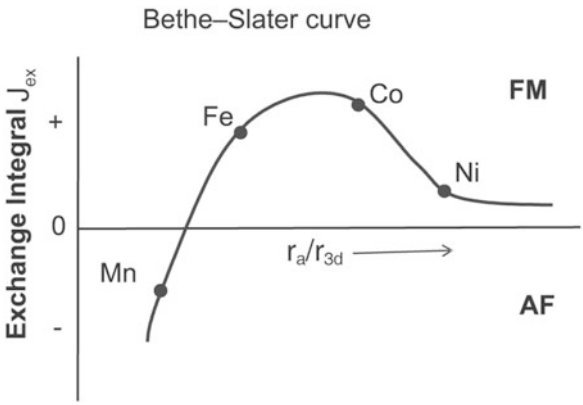

Fig. 8.27 A relation between J_{ex} and interatomic distance for transition elements; Here r_a is interatomic distance and r_{3d} is the radius of 3d shell

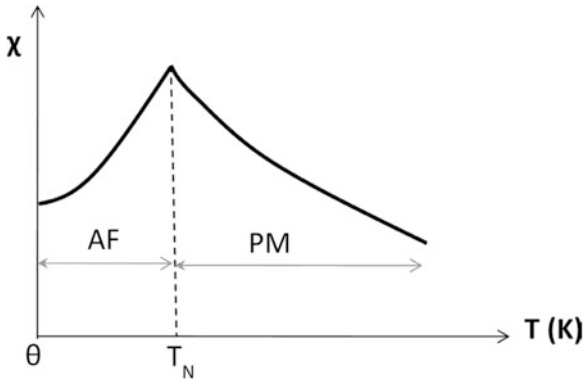

Fig. 8.28 Typical susceptibility curve in case of antiferromagnetic material

Slater showed that there exists a correlation between the interatomic distance and radius of incomplete filled d shell in case of transition elements, which is responsible for the ferromagnetism or antiferromagnetism, as shown in Fig. 8.27. It can be seen that this makes Fe, Co and Ni ($J_{exch} > 0$) ferromagnetic but Mn and Cr ($J_{exch} < 0$) antiferromagnetic materials.

8.5.1.4 Antiferromagnetic Materials

For antiferromagnetic materials the J_{exch} is negative and spins on neighbouring atoms are antiparallel to each other. Susceptibility in these materials is small but positive, as applied magnetic field tends to orient the spins in the direction of magnetic field overcoming the diamagnetism. Figure 8.28 illustrates schematically the susceptibility of antiferromagnetic materials in general.

Antiferromagnetic arrangement exists below a critical temperature known as Néel temperature T_N. Above T_N, susceptibility is paramagnetic and has the form

$$\chi_\theta = \frac{2\chi}{T + T_N} \tag{8.61}$$

8.5.1.5 Ferrimagnetic Materials

As illustrated in Fig. 8.26, there is also ferrimagnetism which is similar to antiferromagnetism but alternate spins are of smaller magnitudes than the rest. In general the ferromagnetic and antiferromagnetic materials are quite complex in their behaviour.

8.5.1.6 Nanomagnetic Materials

With this background of magnetic materials we now proceed to understand properties of some special types of nanomagnetic materials in which materials are reduced at least in one of the dimensions. Magnetic nanoparticles, assemblies of nanoparticles, magnetic nanowires, magnetic thin films or multilayer films and some metal oxide films, doped semiconductor particles or thin films have become the focus of attention due to their interesting magnetoresistive or magnetooptical properties they exhibit. The field of nanomagnetic materials is quite vast and still expanding. We shall discuss some of these materials.

8.5.1.7 Magnetic Nanoparticles

Ferromagnetic materials like Fe, Co, Ni, Fe_3O_4, γ-Fe_2O_3 and many others have very interesting behaviour below a critical size, characteristic of each material. Bulk ferromagnetic materials have spontaneously magnetized domains. Formation of domains occurs in order to minimize the total magnetostatic energy of the system. However below the critical size, domain formation is not energetically favoured and material prefers to be single domain. In such a situation all the spins of atoms are oriented in one direction. Typically, the particles with a size below 100 nm are likely to be single domain. Coercivity H_c in such particles is given by

$$H_c = \frac{2K}{M_s}\left[1 - \frac{T}{T_B}\right] \tag{8.62}$$

where M_s is the saturation magnetization due to applied magnetic field, K – the anisotropy constant and T_B is the blocking temperature. Anisotropy (preferred

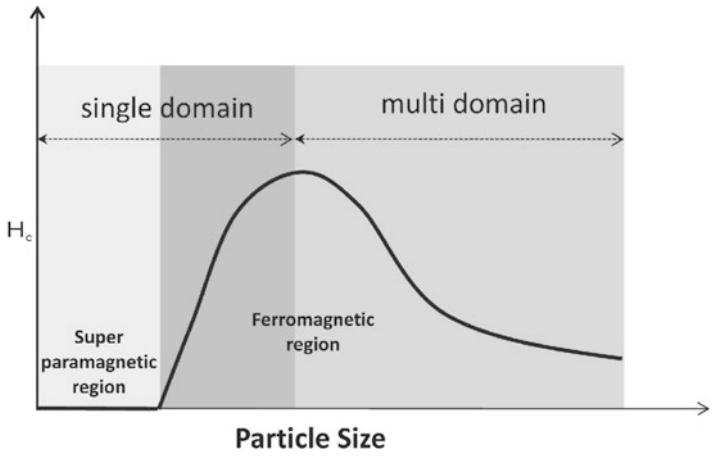

Fig. 8.29 A relation between particle coercivity and size

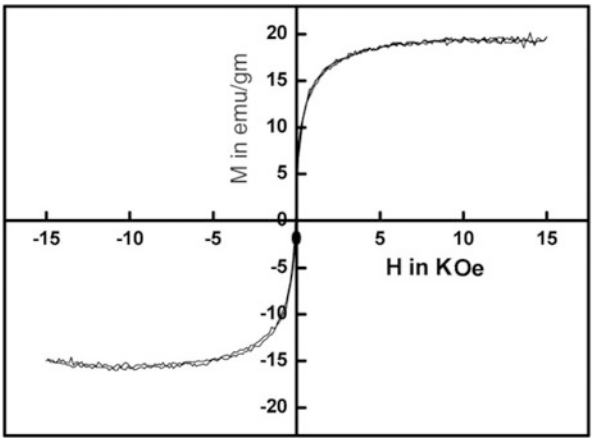

Fig. 8.30 Magnetization behaviour in case of a superparamagnetic particle

orientation of magnetic moments) can arise due to crystal structure, shape, stress and surface. Blocking temperature is the temperature, above which thermal energy is able to set the orientation of magnetic moments free. Below the blocking temperature, they are as if frozen. Figure 8.29 shows a common behaviour in materials of H_c as a size of particles.

Single domain particles of extremely small size which do not show coercivity or hysteresis (see Fig. 8.30) are known as superparamagnetic particles.

In superparamagnetic particles, spins are oriented in one direction and switch coherently in the opposite direction. The switching time is of the order of few nanoseconds and is given by

$$t = \tau_0 e^{-KV/kT} \tag{8.63}$$

where KV is the barrier for total spin orientation. Typical measurements of magnetization require 10–100 seconds. Thus magnetization (M) versus applied field (H) would exhibit the curve as shown in Fig. 8.30 with no coercive field. If magnetization M versus (H/T) are plotted then all the points for a superparamagnetic material lie on a single curve.

Small particles are characterized by large surface to volume ratio. Therefore surfaces and interfaces play an important role in their magnetic properties of nanostructures. At surfaces there is not only the symmetry breaking of the bulk crystal structure but there is a change in the coordination number as well as change in the lattice constant. Such effects can give rise to observation of ferromagnetic behaviour in materials which are not ferromagnetic in the bulk form. The coupling of magnetic nanoparticles spread at short distances also is an interesting area of current research.

8.5.1.8 Magnetic Oxide Materials

Magnetic multilayers are artificially obtained materials in which thin layers of magnetic layers separated by nonmagnetic layers are coupled and show Giant Magneto Resistance (GMR). In some metal oxides it has been observed that some planes are magnetically coupled to each other. This gives rise to huge change in the resistance when magnetic field is applied. The change in resistance is even larger than that in magnetic multilayers and is referred to as Collosal Magnetoresistance or CMR.

Colossal Magnetoresistance has been predominantly discovered in manganese-based perovskite oxides. In these crystals strong mutual coupling of spin and charges on atoms is observed. Hence not only high temperature superconductivity, but also new magnetoelectronic properties are increasingly discovered in materials with perovskite structures.

The 3d transition metal oxides, particularly the manganites are being exploited from the prospects of having improved device performance as compared to the GMR materials. These oxides display a diverse nature of properties such as paramagnetic to ferromagnetic transition accompanied by insulator to metal transition and realization of high magnetoresistance on application of comparatively low magnetic field. Historically magnetoresistance in manganites is known since 1950s. But recent interest is developed in doped manganites for exploring further high magnetoresistance value at room temperature at low magnetic field value to interplay of spin, charge and lattice distortion.

For example, undoped $LaMnO_3$ is an antiferromagnetic charge transfer insulator wherein Mn is in $+3$ valence state. As shown in Fig. 8.31 it has a perovskite structure. If any divalent atom (such as Ca, Sr, Ba, Pb) is doped at La site for instance, $La_{1-x}Ca_xMnO_3$, it converts Mn^{+3} to Mn^{+4} state in equal proportion of the doping concentration. This is equivalent to the hole doping in the system. The hole doping introduces a number of dramatic changes in electric and magnetic

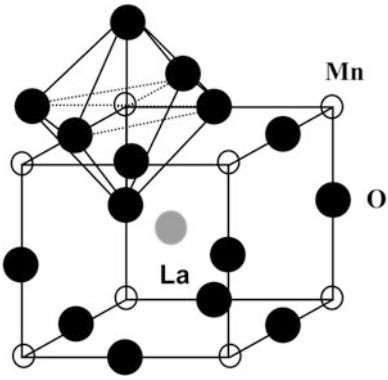

Fig. 8.31 Perovskite structure of $LaMnO_3$

properties from the parent $LaMnO_3$ compound, such as insulator-metal transition, paramagnetic-ferromagnetic transition, charge ordered state, phase separation etc. In the light of these rich physical properties, hole doped $LaMnO_3$ has a potential for promising device applications such as magnetic sensors, magnetic valves, read head technology and bolometric application. Thin films of these materials are therefore a topic of great current interest.

8.6 Mechanical Properties of Nanomaterials

Mechanical properties of materials depend upon the composition and bonds between the atoms viz. covalent, ionic, metallic etc. As a result purest materials may be inherently weak or strong or brittle. Presence of impurities affects all these properties. Most of the materials have various impurities like C, O, N, P, S etc. present in them as well as point defects, grain boundaries, dislocations etc., which are responsible for the deviations of the properties expected from high purity and ordered materials.

When the size of materials is reduced to nanoscale, materials tend to be single crystals. However we need to consider different types of nanomaterials as schematically illustrated in Fig. 8.32 to specify the properties.

Indeed it is possible to determine various mechanical properties like elasticity, hardness, ductility etc. of different nanostructures. Techniques like bending measurement, velocity of sound measurement, nanoindentation etc. can be used. It should be, however, noted that measurements on single nanoparticles, rods, tubes etc. would inherently be difficult, though not impossible. However measurements on nanocrystalline solids, thin films etc. are possible using some conventional methods.

It has been shown in case of metallic nanocrystalline materials (as in Table 8.4) that elastic modulii reduce dramatically. For example in case of magnesium nanocrystalline material (grains $\sim$12 nm size), Young's modulus was observed to be 3,900 N/mm^2 as against 4,100 N/mm^2 for polycrystalline (size >1 μm)

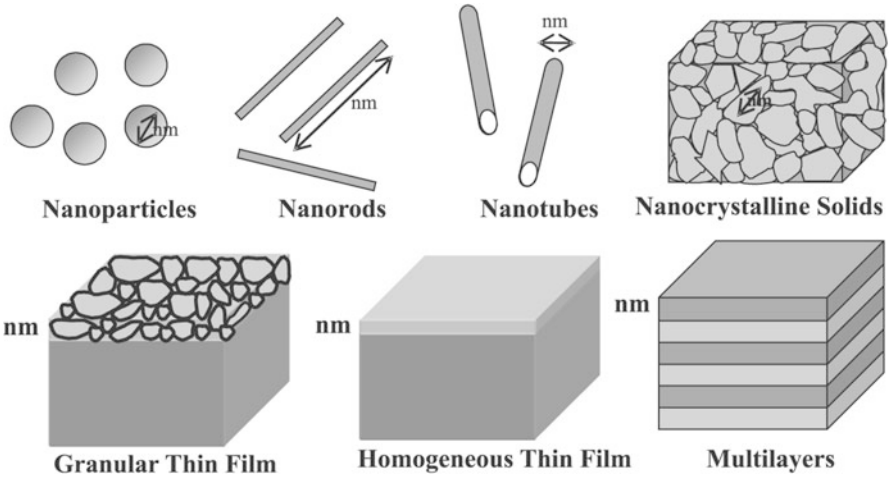

Fig. 8.32 Some common types of nanocrystalline materials

Table 8.4 Elastic properties of some common materials

Material	Density kg/m^3	Young's modulus 10^9 N/m^2
Steel	7,860	200
Al	2,710	70
Glass	2,190	65
Concrete	2,320	25–35
Bone	1,900	9
Polystyrene	1,050	3
Diamond	3,510	1,035
CNT	2,600	1,280

magnesium. In case of palladium, nanocrystallites of ∼8 nm size had Young's modulus 8,800 N/mm^2 as against 12,300 N/mm^2 for polycrystalline palladium.

Ceramic materials are often compacted and sintered using powder material. This also increases the hardness of materials. It has been shown that in case of TiO_2 nanoparticles (∼12 nm size) produced in powder form much less temperature was required to densify and achieve the hardness comparable to usual polycrystalline material.

In fact density of nanocrystalline pellet is often low due to some pores left when powders are compressed to form pellets. Nanocrystalline pellets densities approach those of bulk polycrystalline materials as the sintering at high temperature progresses.

Plastic deformation in nanocrystalline materials strongly differs from that of polycrystalline bulk counterpart as shown in Fig. 8.33. It was shown in case of nickel that stress removal results in more effective recovery of the material as compared to corresponding polycrystalline material.

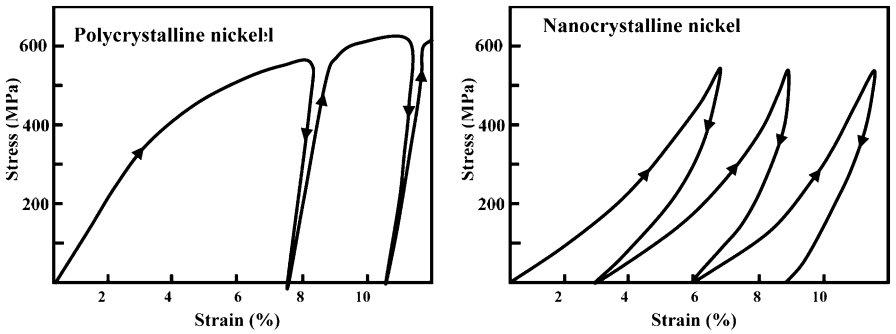

Fig. 8.33 Comparison of stress and strain relation in case of nanocrystalline and polycrystalline material

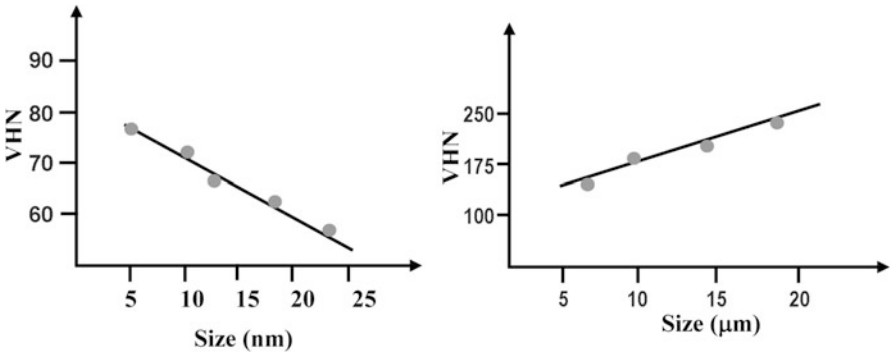

Fig. 8.34 Hardness variation for copper in nanometer and micrometre grain size range

Hardness of materials is also related to the grain size. As illustrated in Fig. 8.34 for copper, even in micrometre grain size range there is a linear dependence of hardness on particle size. It decreases with increase of grain size. However in nanometer size range, the hardness increases with increase of particle size linearly. Similar results are found in case of palladium nanoparticles and microparticles.

8.7 Structural Properties

Even though some nanomaterials with slightly large number of atoms (>50–60 atoms) may acquire bulk crystalline structure, it is found that the lattice parameters may not be the same as in the bulk material. For example it has been shown by rigorous analysis of X-ray diffraction patterns of ZnS that as small as 1.4 nm particles had liquid disorder. However larger crystals of ZnS indeed show same

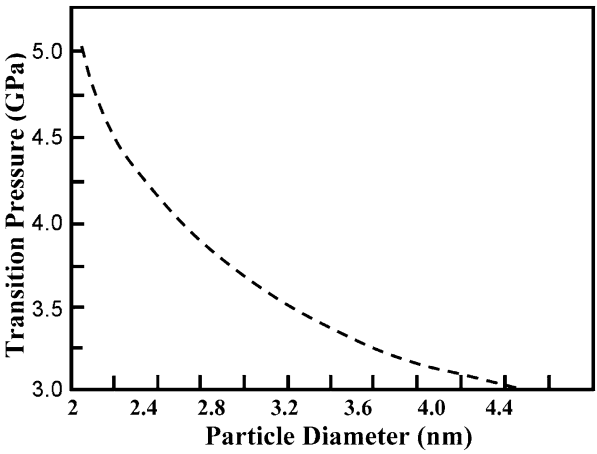

Fig. 8.35 Structural deformation of CdSe nanoparticles

sphalerite (cubic) structure as in the bulk. It has been observed that there is a lattice contraction of ∼1 % for 1.4 nm ZnS nanoparticles. Other small particles also show up to ∼2–3 % lattice constant deviations compared to bulk crystalline materials.

With increase in temperature the disordered structure of small particles of ZnS were found to transform to wurtzite (hexagonal) structure. Further the chemical capping, often used in the synthesis of nanoparticles, gets removed and particles tend to agglomerate or coalesce forming larger particles.

Effect of pressure on structural properties (using X-ray diffraction) has also been well investigated for some nanoparticles. It has been found that indeed the structural transformations do take place in case of nanoparticles with applied pressure. However the pressures required for this are larger for nanoparticles than for corresponding bulk material and depend upon the particle size, as illustrated in Fig. 8.35 for CdSe nanoparticles. Thus CdSe nanoparticles of 1–2.1 nm required 4.9 GPa to 3.6 GPa pressure to transform them from wurtzite to rock salt structure. Bulk CdSe needs just 2.0 GPa for the same transformation.

8.8 Melting of Nanoparticles

A variety of nanoparticles like Au, Ag, CdS etc. have been investigated for their thermal stability and melting. Melting begins at the surface. As the particle size decreases surface to bulk atoms ratio increases dramatically. In small particles or clusters the central atom may be considered as surrounded by 1st, 2nd, 3rd, ... compact shells of atoms. Number of atoms in shells is given as $10\,n^2 + 2$. Thus 1st shell would have 12 atoms, 2nd shell would have 42 atoms and so on. It can be easily seen that number of surface atoms is quite large in nanoparticles and surface to bulk atoms ratio goes on increasing with decreasing particle size (or shells). Large surface

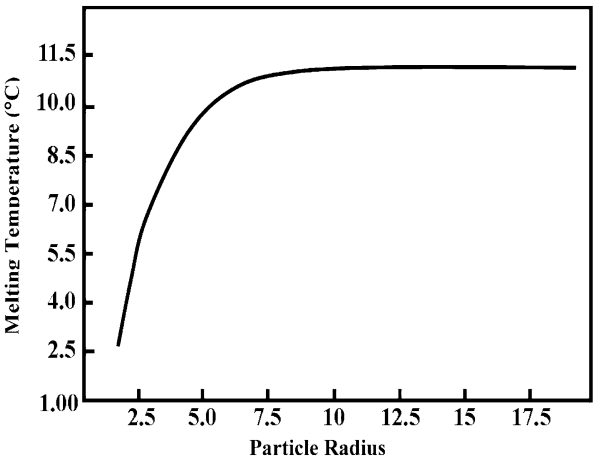

Fig. 8.36 Variation of melting point with size of nanoparticles

is related to large surface energy. This energy can be lowered by melting. As shown in Fig. 8.36 melting temperature of gold nanoparticles of 3–4 nm size is reduced by ~500 °C compared to bulk melting point.

Melting of nanoparticles is usually determined either by X-ray diffraction or electron diffraction. Heating increases the lattice parameter and at melting long range order is lost.

Further Reading

M. Born, E. Wolf, *Principles of Optics* (Cambridge University Press, Cambridge, 2003)
W.D. Callister, *Materials Science and Engineering: An Introduction*, 4th edn. (Wiley, New York, 1997)
M. Fox, *Optical Properties of Solids* (Oxford University Press, Oxford, 2012)
H. Gleiter, Nanocrystalline materials. Prog. Mater. Sci. **33**, 227 (1989)
S. Shionoya, W.M. Yen (eds.), *Phosphor Handbook* (CRC Press, Boca Raton, 1999)